universe

IMPACT FACTOR 2.9

CITESCORE 3.6

Review

Asteroseismology of Compact Stars

Hong-Bo Li, Yong Gao, Lijing Shao and Ren-Xin Xu

Special Issue
Pulsar Astronomy

Edited by
Prof. Dr. Wei Wang and Prof. Dr. Renxin Xu

MDPI

https://doi.org/10.3390/universe10040157

universe

MDPI

Review

Asteroseismology of Compact Stars

Hong-Bo Li [1,2,*], Yong Gao [3], Lijing Shao [2,4] and Ren-Xin Xu [1,2]

[1] Department of Astronomy, School of Physics, Peking University, Beijing 100871, China; r.x.xu@pku.edu.cn
[2] Kavli Institute for Astronomy and Astrophysics, Peking University, Beijing 100871, China; lshao@pku.edu.cn
[3] Max Planck Institute for Gravitational Physics (Albert Einstein Institute), Am Mühlenberg 1, 14476 Potsdam, Germany; gaoyong.physics@pku.edu.cn
[4] National Astronomical Observatories, Chinese Academy of Sciences, Beijing 100012, China
* Correspondence: lihb2020@stu.pku.edu.cn

Abstract: Compact stars have been perceived as natural laboratories of matter at an extremely high density. The uncertainties of the equation of state (EOS) of matter can be constrained by observing compact stars. In this review, we investigate the EOSs, global structure, and elastic properties of compact stars. We focus in detail on how to constrain the above properties of compact stars via asteroseismology. Observations that include studies of quasi-periodic oscillations from giant flares of soft gamma-ray repeaters and gravitational waves provide information about the elastic properties and internal compositions of compact stars.

Keywords: asteroseismology; compact stars; oscillations; gravitational waves

1. Introduction

The equation of state (EOS) for dense matter holds a crucial role in many astrophysical phenomena linked to neutron stars (NSs). Given the non-perturbative properties of strong interaction at low energy, the EOS stands as a key question in both astrophysics and nuclear physics [1–3]. The EOS can also be used to infer key aspects of microphysics, such as the role of many-body interactions at nuclear densities. At high densities, one expects transitions to non-nucleonic states of matter [4], such as the formation of hyperons, and free quarks. The entire star may convert into a lower energy self-bound state consisting of u, d, and s valence quarks, known as a strange quark star (QS) [5], or a strangeon star (SS) [6], the latter of which could be in a solid state due to massive strangeons and to low temperatures. Other states that have been hypothesized include Bose–Einstein condensates of mesons [7] or strange quark matter that may form superfluid in the core of NSs, giving rise to hybrid stars (HSs) [8], and even hybrid strangeon stars [9]. Differently, the conventional NSs and HSs are gravity-bound models, while QSs and SSs are self-bound models with strong interaction.

Besides magnetospheric activity [10] and gravitational-wave echoes [9], elastic properties play also an important role in identifying the nature of compact stars, which is the focus of this paper. The investigation of the solid crust properties of NSs has garnered significant attention. This is because vibrations within the crust could offer a mechanism for the quasi-periodic oscillations (QPOs) observed in the giant flares (GFs) of soft gamma-ray repeaters (SGRs) [11,12]. The problem of mountain formation on the surface of NSs is connected to their elastic properties. These mountains can be efficient sources of continuous gravitational waves (CGWs) [13–17]. The starquake model [18] and the superfluid component of NSs [19–21] can explain the pulsar glitches [22]. On the other hand, involving the SS model may illuminate the physical mechanisms behind pulsar glitches [23–26] and the QPOs in GFs [27].

It is worth noting that NS observations could find observable signatures and test predictions from theoretical models. Measurements of the masses or radii of NSs can strongly constrain the EOS and consequently the interior composition of NSs. Pulsar

check for updates

Citation: Li, H.-B.; Gao, Y.; Shao, L.; Xu, R.-X. Asteroseismology of Compact Stars. *Universe* **2024**, *10*, 157. https://doi.org/10.3390/universe10040157

Academic Editor: Nicolas Chamel

Received: 12 January 2024
Revised: 19 March 2024
Accepted: 24 March 2024
Published: 27 March 2024

timing obtains the cleanest constraints on the EOS and the most massive pulsars have masses $M \approx 2\,M_{\odot}$ [28,29]. The Neutron Star Interior Composition Explorer (NICER) experiment is currently measuring the mass and radii of several NSs [30–36]. Moreover, the tidal deformability of a compact star carries important information about the EOS of the star. The observation of the GW170817 event set an upper limit on the NS tidal Love number $\tilde{\Lambda} \leq 800$, which ruled out some stiff EOSs [37]. Yunes et al. [38] discussed how to provide interior information on the NS combined gravitational waves (GWs) with X-ray observations.

Certainly, pulsating compact stars are important sources of information for astrophysics, which would greatly constrain basic properties like the EOS, or crust elasticity. Non-axisymmetric stellar oscillations will lead to the production of gravitational radiation [39,40]. A realistic NS model has rich oscillation spectra with various modes. For typical non-rotating relativistic stars, various modes are classified in polar and axial categories. Note that the two classes of modes are often called spheroidal and torsional in Newtonian stellar pulsation. The spheroidal modes include the fundamental (f) modes, pressure (p) modes, and gravity (g) modes. The torsional modes have spacetime (w) modes, which are directly associated with the spacetime metric [41], and the shear (s) modes, which depend on the shear modulus [42]. In this review, we focus in detail on asteroseismology, which aims to constrain the EOSs, global structure, and elastic properties of compact stars, and how the results may impact observations, in particular, related to QPOs in GFs and GW observations.

An exciting possibility is the existence of quark matter at high densities [43]. The features in the EOS can also be inferred from GW observations through tides. Such tidal deformability can be used to probe a quark matter core [43–46]. Moreover, the existence of a possible hadron–quark phase transition at high densities is associated with the appearance of a g-mode and interfacial (i)-mode. The potential detectability of g-modes in various NS models with different compositions uses third-generation GW detectors by stacking multiple events [47]. Lau and Yagi [48], Zhu et al. [49] investigated the dynamical tides of the i-mode associated with a quark-hadron phase transition. These results indicate that a ground-based GW detector has the potential to detect the signature of these phase transitions via the crust–core interfacial mode.

The paper is organized as follows. In Section 2, we review the EOSs of NSs, QSs, and SSs. In Section 3, we review the global aspects of NSs, QSs, and SSs, including the mass–radius relations and the maximum mass versus the corresponding central density. The elastic properties of compact stars are reviewed in Section 4. The asteroseismology of compact stars is presented in Section 5. The radial oscillation modes and the dynamical stability are discussed in Section 5.1. The relation between spheroidal oscillation modes and tidal deformability is studied in Section 5.2. Observations of oscillations in GFs from SGRs are confronted with models of torsional oscillations in Section 5.3.

2. Equation of State of Compact Stars

2.1. Neutron Star

In this subsection, we will summarize the NS interiors in detail. The stellar structure can be roughly divided into four distinct sections: the atmosphere, the outer crust, the inner crust, and the core [7].

The atmosphere is a thin plasma layer, situated on the uppermost layer of a star. It contains a negligible amount of mass, but it plays an important role in shaping the outgoing radiation. In particular, the radiation emitted by NSs gives information on the parameters of the surface layer, the effective surface temperature, surface gravity, chemical composition, and cooling [50,51].

The crust extends for about 1–2 km on the top of the core and is typically divided into an outer and inner layer. The outer crust extends from the atmosphere bottom to the layer of the neutron drip density (i.e., $\rho \approx 4 \times 10^{11}\,\mathrm{g\,cm^{-3}}$). The characteristics of the matter are strongly dependent on the Coulomb interactions of charged particles that form a solid

Coulomb crystal. Matter at densities below neutron drip is not only relevant for outer crusts of NSs but also for white dwarfs. Following Baym et al. [52], the total energy density can be written as

$$\rho_{\rm tot} = n_{\rm N} E\{A, Z\} + \rho_e + \rho_L \,, \tag{1}$$

where $n_{\rm N}$ is the number density of nuclei, $E\{A, Z\}$ is the energy of a nucleus with Z protons and $A - Z$ neutrons, and ρ_e is the electron kinetic energy density,

$$\rho_e = \frac{m_e c^2}{\lambda_e^3}\left\{x(1+x^2)^{1/2}(1+2x^2) - \ln[x + (1+x^2)^{1/2}]\right\}, \tag{2}$$

where λ_e is the electron Compton wavelength, $x = p_F/m_e c$ is a dimensionless relativity parameter, p_F is the Fermi momentum, and the ρ_L is the lattice energy density, which accounts for the electron–electron, electron–ion, and ion–ion Coulomb interactions, which are determined as

$$\rho_L = -\frac{9}{10}\left(\frac{4\pi}{3}\right) Z^{2/3} e^2 n_e^{4/3} \,, \tag{3}$$

where n_e is the number density of the electron. According to the first law of thermodynamics, the total pressure P is given by

$$P = n_{\rm b}^2 \frac{\rm d}{{\rm d}n_{\rm b}}\left(\frac{\rho_{\rm tot}}{n_{\rm b}}\right), \tag{4}$$

where n_b is the baryon number density. Moreover, using Equation (1), the total pressure P can be expressed as

$$P = P_e + \frac{1}{3}\rho_L \,. \tag{5}$$

Here, the electron pressure $P_e = \rho_e - \mu_e n_e$, where μ_e is the electron chemical potential.

The inner crust is taken to continue down to the crust–core interface, where density extends from $\rho \approx 4 \times 10^{11}\,{\rm g\,cm^{-3}}$ to $\rho \approx 2.8 \times 10^{14}\,{\rm g\,cm^{-3}}$. The matter of the inner crust may condense into a superfluid phase [7,53–55]. The structure of the inner crust has been studied using different approximations and nuclear models [54]. Moreover, the EOSs of the inner crust have been described by parametrized polytrope models. For example, the analytic form of the SLy EOS is set by the values of the coefficient K_i, the adiabatic index Γ_i, and the rest-mass density ρ_i listed in Table II of Read et al. [56]. At the bottom of the crust, some calculations predict various pasta phases of nonspherical nuclei, such as slab-like or cylinder phases [57].

The core constitutes up to 99 % of the NS mass. A density range between $1.4 \times 10^{14}\,{\rm g\,cm^{-3}}$ and $5.6 \times 10^{14}\,{\rm g\,cm^{-3}}$ corresponds to the outer core [7]. The matter consists of neutrons; protons; electrons; and in some models, muons. This matter is determined by charge neutrality, β-equilibrium, and many-body nuclear interactions. Beyond $\rho > 5.6 \times 10^{14}\,{\rm g\,cm^{-3}}$, it is called the inner core, and its composition is even more unknown. Hence, the results here become sensitively model-dependent. The models have hyperonization (Σ^- and Λ), pion condensation (π), kaon condensation (K), or even a phase transition to a quark matter. Quark matter may form the crystalline color superconducting (CSC) phase at the core of NSs, giving rise to HSs [8]. Haskell et al. [58] estimated the maximal deformation that can be sustained by rotating HSs. Probing elastic quark phases in HSs with radius measurements has been discussed by Pereira et al. [59].

A phenomenological model parameterizes those EOSs in contrast to describe the accurate but complicated microphysics. Read et al. [56] calculated a piecewise polytropic description of the EOSs, and the method of the spectral representations has been discussed by Lindblom [60].

2.2. Quark Star

If we consider noninteracting quark matter, it takes into account the bare quark kinetic energy density, ρ_K, and the bag constant, B, which is the energy density difference between

the nonperturbative vacuum in quantum chromodynamics (QCD) and the perturbative vacuum [2]. We consider several massless quarks with N_f flavors. The quarks form a degenerate Fermi sea at low temperatures, and the quark number density is given by

$$n_q = 2N_c N_f \int_0^{p_F} \frac{d^3p}{(2\pi)^3} = N_c N_f \frac{p_F^3}{3\pi^2}\,, \tag{6}$$

where $N_c = 3$ is the number of quark colors, and p_F is the quark Fermi momentum. The bare quark kinetic energy density is defined by

$$\rho_K = 2N_c N_f \int_0^{p_F} \frac{d^3p}{(2\pi)^3}|p| = \frac{N_c N_f}{4\pi^2} p_F^4\,. \tag{7}$$

The total energy density is $\rho = \rho_K + B$, and the baryon chemical potential $\mu_B = 3\mu_q$, where $\mu_q = \partial\varepsilon/\partial n_q$ is the quark chemical potential. Hence, the energy density and pressure can be represented as

$$\rho(p_F) = 3ap_F^4 + B\,, \tag{8}$$

$$P(p_F) = ap_F^4 - B\,, \tag{9}$$

where $a = N_c N_f/(12\pi^2)$. The maximum mass of the QS scales with B as [2]

$$M_{\max} \simeq 1.78 \left(\frac{155\,\mathrm{MeV}}{B^{1/4}}\right)^2 M_\odot\,, \tag{10}$$

and the corresponding radius scales as

$$R \simeq 9.5 \left(\frac{155\,\mathrm{MeV}}{B^{1/4}}\right)^2 \mathrm{km}\,. \tag{11}$$

As described in the Introduction, the QS is a self-bound model, and the pressure vanishes at a nonvanishing value of the energy density.

Deconfined quarks at low-temperature and high-density regimes can form a condensate of Cooper pairs driven by the BCS mechanism [61] and become CSC [62]. We follow the phenomenological quark-matter EOS model [8]. The model is based on the thermodynamic potential

$$\Omega_{\mathrm{QM}} = -\frac{3}{4\pi^2} a_4 \mu_q^4 + \frac{3}{4\pi^2} a_2 \mu_q^2 + B_{\mathrm{eff}}\,, \tag{12}$$

where the parameters a_4, a_2, and B_{eff} are independent of μ_q. The reasonable value for a_4 is expected to be of order 0.7 [8] and $a_4 = 1$ for the model of the free non-interacting quarks. The parameter a_2 is used to model the effects of quark masses and pairing, and B_{eff} is an effective bag constant. The energy density and pressure are given by

$$\rho = \frac{9}{4\pi^2} a_4 \mu_q^4 - \frac{3}{4\pi^2} a_2 \mu_q^2 + B_{\mathrm{eff}}\,, \tag{13}$$

$$P = \frac{3}{4\pi^2} a_4 \mu_q^4 - \frac{3}{4\pi^2} a_2 \mu_q^2 - B_{\mathrm{eff}}\,. \tag{14}$$

In Figure 1, we show the relations of the pressure and the energy density against quark chemical potential for the CSC model. Moreover, Lin [63] investigated the torsional oscillations of HSs with crystalline CSC. Lau et al. [64] studied the tidal deformability of HSs with crystalline CSC, and the deviations of the tidal deformability from the fluid case are in the order of 10 %.

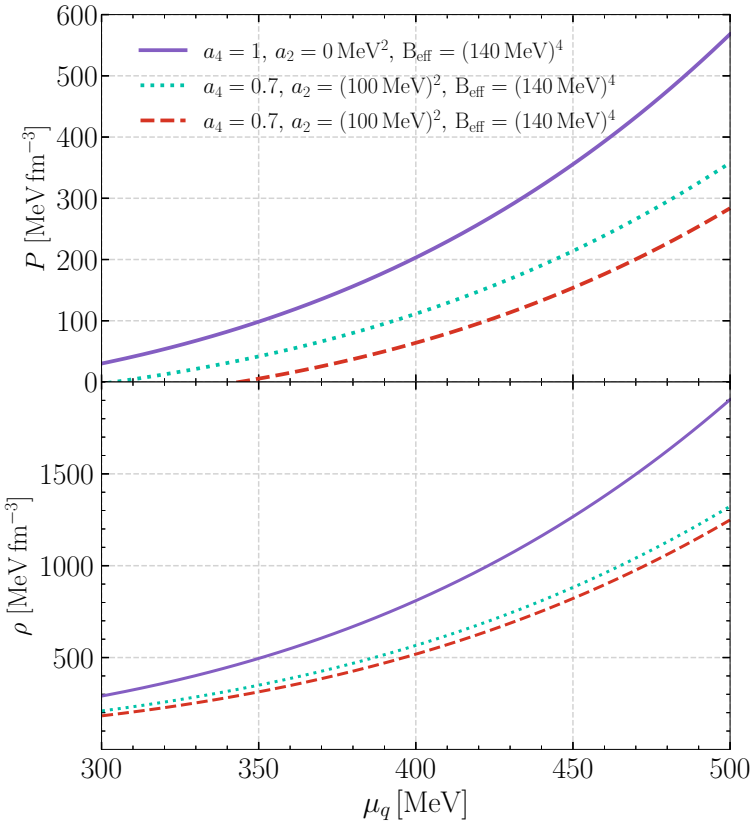

Figure 1. The upper panel shows the pressure as a function of the quark chemical potential μ_q. The lower panel shows the relationship between the energy density and the quark chemical potential μ_q.

2.3. Strangeon Star

In view of the non-perturbative strong interaction between three-flavoured quarks at free pressure, as in the case of two-flavoured atomic nuclei, Xu [6] conjectured that the bulk dense matter may be composed of strangeons, which are quark clusters with nearly equal numbers of u, d, and s valence quarks, rather than a CSC phase. The interaction potential between two strangeons could be Lennard-Jones-like in analogy to the case of condensed matter made of chargeless atoms, to be described by the 6–12 potential,

$$u(r) = 4\epsilon\left[\left(\frac{\sigma}{r}\right)^{12} - \left(\frac{\sigma}{r}\right)^{6}\right], \tag{15}$$

where ϵ is the depth of the potential, r is the distance between two strangeons, and σ is the distance when $u(r) = 0$. We note that this potential exhibits a characteristic of repulsion at short distances and attraction at long distances.

Based on the findings from earlier investigations [65–67], the potential energy density is given by

$$\rho_{\mathrm{p}} = 2\epsilon\left(A_{12}\sigma^{12}n^5 - A_6\sigma^6 n^3\right), \tag{16}$$

where $A_{12} = 6.2$, $A_6 = 8.4$, and n is the number density of strangeons. The total energy density of zero-temperature dense matter composed of strangeons reads

$$\rho = 2\epsilon\left(A_{12}\sigma^{12}n^5 - A_6\sigma^6 n^3\right) + nN_{\mathrm{q}}m_{\mathrm{q}}, \tag{17}$$

where $N_{\rm q} m_{\rm q}$ is the mass of a strangeon with $N_{\rm q}$ being the number of quarks in a strangeon and $m_{\rm q}$ being the quark mass. From the first law of thermodynamics, one derives the pressure

$$P = n^2 \frac{{\rm d}(\rho/n)}{{\rm d}n} = 4\epsilon\left(2A_{12}\sigma^{12}n^5 - A_6\sigma^6 n^3\right). \tag{18}$$

At the surface of SSs, the pressure becomes zero and we obtain the surface number density of strangeons as $\left[A_6/(2A_{12}\sigma^6)\right]^{1/2}$. For convenience, we transform it to the number density of baryons

$$n_{\rm s} = \left(\frac{A_6}{2A_{12}}\right)^{1/2} \frac{N_{\rm q}}{3\sigma^3}. \tag{19}$$

Finally, the EOS can be rewritten into a form that depends on parameter set (ϵ, n_s, N_q):

$$\rho = \frac{1}{9}\epsilon\frac{A_6^2}{A_{12}}\left(\frac{{N_q}^4}{18n_s^4}n^5 - \frac{N_q^2}{n_s^2}n^3\right) + m_q N_q n\,, \tag{20}$$

$$p = \frac{2}{9}\epsilon\frac{A_6^2}{A_{12}}\left(\frac{N_q^4}{9n_s^4}n^5 - \frac{N_q^2}{n_s^2}n^3\right). \tag{21}$$

Recently, Zhang et al. [9] removed the parameters n_s and N_q by doing the following dimensionless rescaling:

$$\bar{\rho} = \frac{\rho}{m_q\, n_s}\,, \quad \bar{p} = \frac{p}{m_q\, n_s}\,, \quad \bar{n} = \frac{N_q\, n}{n_s}\,, \quad \bar{\epsilon} = \frac{\epsilon}{N_q\, m_q}\,, \tag{22}$$

so that

$$\bar{\rho} = \frac{a}{9}\bar{\epsilon}\left(\frac{1}{18}\bar{n}^5 - \bar{n}^3\right) + \bar{n}\,, \tag{23}$$

$$\bar{p} = \frac{2\,a}{9}\bar{\epsilon}\left(\frac{1}{9}\bar{n}^5 - \bar{n}^3\right), \tag{24}$$

where $a = A_6^2/A_{12} \approx 11.38$. In particular, we observe that the three parameters (n_s, ϵ, N_q) can be reduced to a single parameter ($\bar{\epsilon}$).

SSs can explain many observational phenomena in astrophysics, including pulsar glitches, sub-pulse drifts, the presence of extremely strong magnetic fields, and the transient bursts of GCRT J1745−3009 [10,23,68–71], even for fast radio bursts related to galactic magnetars [72,73]. The tidal deformability of merging binary SSs, along with the analysis of ejecta and light curves, has been investigated in previous works [74–76]. Recently, Gao et al. [77] have explored the universal relations among the moments of inertia I, the tidal deformability λ, and the quadrupole moment Q of SSs.

In the upper panel of Figure 2, we summarized the density and pressure relations for these EOSs. One notices that there is a large difference between different EOS models, especially between the models for a conventional NS and models for a QS or an SS. This characteristic remains valid approximately as the mass of the star increases, resulting in distinctions in other aspects such as the moment of inertia [77] and the frequency of oscillation mode [78].

Another important dimensionless parameter characterizing the stiffness of the EOS at a given density is the adiabatic index, defined by

$$\Gamma = \frac{\rho + P}{P}\frac{{\rm d}P}{{\rm d}\rho}\,, \tag{25}$$

which is equal to the adiabatic index governing the equilibrium pressure–energy density relation. In the lower panel of Figure 2, we show that the relation between the adiabatic index Γ and the energy density ρ. It is evident that the adiabatic indices for QSs and SSs

exhibit qualitative differences from those of NSs at low density. Furthermore, SSs generally demonstrate a higher adiabatic index compared to both NSs and QSs, suggesting that the EOSs for SSs are stiffer.

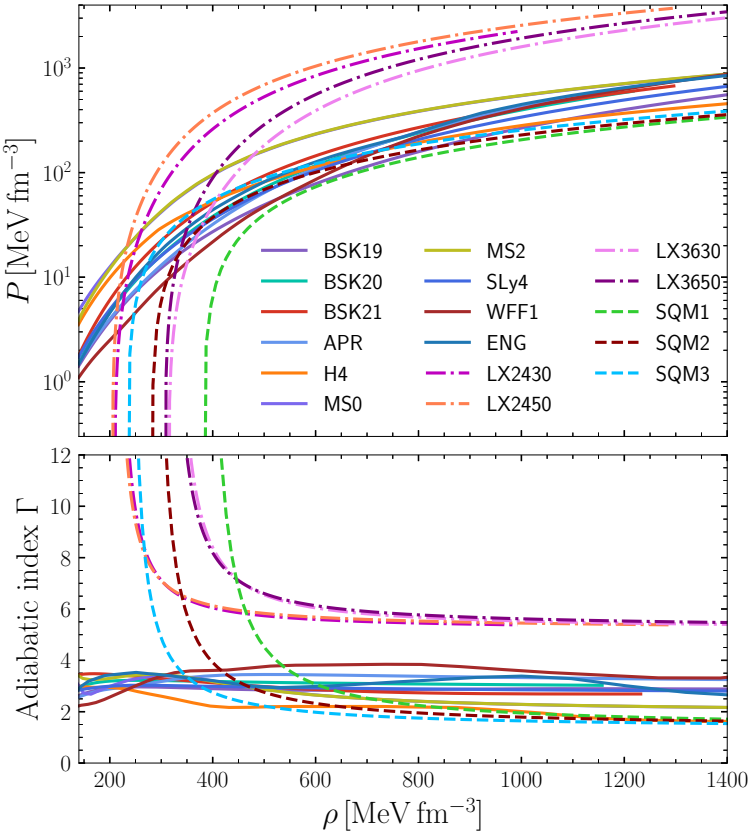

Figure 2. The upper panel shows the relation between mass–energy density ρ and pressure P for NSs [79,80], QSs, and SSs (see Figure 1 in Gao et al. [77]). The lower panel shows the adiabatic index Γ as a function of the mass-energy density ρ. We represent the EOSs of SSs through their corresponding values of n_s and ϵ. For instance, the label "LX2430" signifies a surface baryon number density of $n_s = 0.24\,\mathrm{fm}^{-3}$ and a potential depth of $\epsilon = 30\,\mathrm{MeV}$. "SQM" is related to QSs in the MIT bag model [79].

3. Global Structure of Compact Stars

Global aspects of compact stars are determined by the equations of hydrostatic equilibrium. In this section, we will discuss the basic information of a compact star, revealing the interaction and inner structure of its components. In the following, we take $G = c = 1$ except when the units are written out explicitly, and the convention of the metric is $(-,+,+,+)$.

We shall consider an unperturbed star to be composed of a perfect fluid. The energy-momentum tensor is $T^{\mu\nu} = (\rho + p)u^\mu u^\nu + pg^{\mu\nu}$. The static and spherically symmetric metric, which describes an equilibrium relativistic star is given by the line element,

$$\mathrm{d}s^2 = -e^{2\Phi}\mathrm{d}t^2 + e^{2\Lambda}\mathrm{d}r^2 + r^2(\mathrm{d}\theta^2 + \sin^2\theta\mathrm{d}\phi^2)\,, \tag{26}$$

where Φ and Λ are metric functions of r. A mass function $m(r)$ is defined as $m(r) = r(1 - e^{-2\Lambda})/2$, which satisfies

$$\frac{\mathrm{d}m}{\mathrm{d}r} = 4\pi r^2\rho\,, \tag{27}$$

where ρ is the mass-energy density. The Tolman–Oppenheimer–Volkoff (TOV) equations that determine the pressure $P(r)$ and the metric function $\Phi(r)$ are expressed as

$$\frac{\mathrm{d}P}{\mathrm{d}r} = -(\rho + P)\frac{\mathrm{d}\Phi}{\mathrm{d}r}, \tag{28}$$

$$\frac{\mathrm{d}\Phi}{\mathrm{d}r} = \frac{m + 4\pi r^3 P}{r(r - 2m)}. \tag{29}$$

Integrating Equations (27)–(29) combined with the EOSs, which are described in Figure 2, one obtains the stellar structure of spherical stars and the corresponding spacetime geometry. In Figure 3, we show the mass–radius relations for NSs, QSs, and SSs using the aforementioned EOSs.

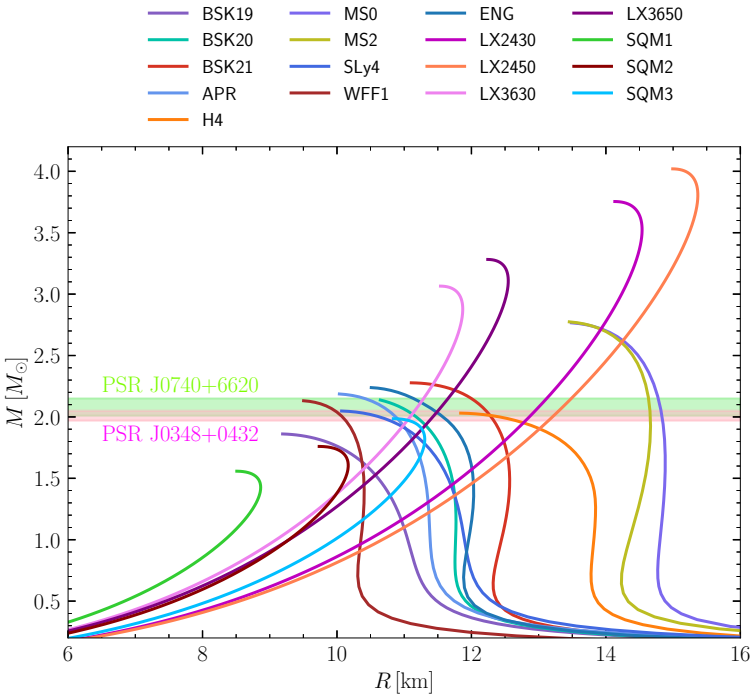

Figure 3. Mass-radius relations of NSs, QSs, and SSs [77]. The 1-σ regions of the mass measurements in PSRs J0348+0432 [28] and J0740+6620 [29] are illustrated.

The maximum mass of NSs serves as an indicator of the stiffness of high-density EOSs. The observation of massive NSs around $2M_\odot$ through pulsar timing has ruled out extremely soft EOSs [28,29]. Lattimer and Prakash [81] demonstrated that the largest measured NS mass can also establish an upper bound to the energy density of cold baryonic matter. As shown in Figure 4, a larger maximal mass M_{TOV} corresponds to a lower central density ρ_{c}. Hence, a sufficiently large measured mass could rule out classes of possible EOSs. The upper limit of the central density will be revised downwards if more massive NSs are discovered in the future, potentially challenging the applicability of perturbative QCD in proposing the existence of a quark phase within NS cores [82–86].

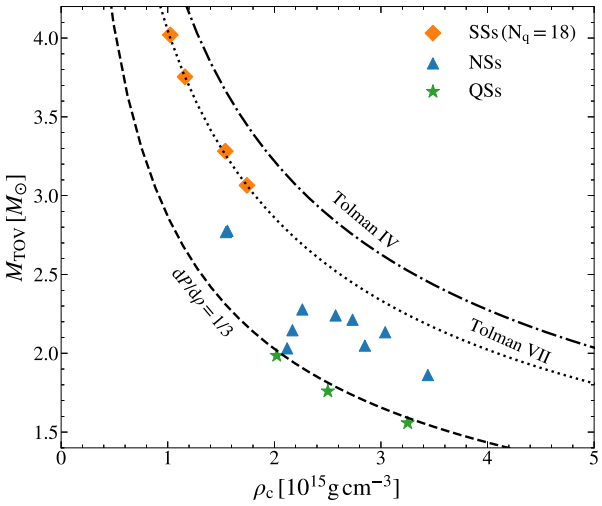

Figure 4. The relation between the maximum mass $M_{\rm TOV}$ and the corresponding central density $\rho_{\rm c}$ (see Figure 3 in Gao et al. [77]). Results for different classes of EOSs shown in Figure 2 are depicted: SSs (*diamond*), conventional NSs (*triangle*), and QSs in the MIT bag model (*star*). The $M_{\rm TOV}$–$\rho_{\rm c}$ relation for $\mathrm{d}P/\mathrm{d}\rho = 1/3$ as well as the Tolman IV and Tolman VII solutions coupled with $\mathrm{d}P/\mathrm{d}\rho = 1$ are illustrated. The Tolman solutions approximately bound all studied EOSs, and the curve $\mathrm{d}P/\mathrm{d}\rho = 1/3$ effectively bounds stars containing free quarks.

4. Elastic Properties of Compact Stars

The study of the elastic properties of the crust is a crucial aspect in the physics of NSs. Chamel and Haensel [54] have summarized the elastic properties of the NS crust. Elastic properties of an isotropic solid are described by two elastic moduli. The deformation energy can be written as

$$\varepsilon_{\rm def} = \frac{1}{2}K(\boldsymbol{\nabla}\cdot\boldsymbol{u})^2 + \mu\left[u_{ik} - \frac{1}{3}\delta_{ik}\,(\boldsymbol{\nabla}\cdot\boldsymbol{u})\right]^2, \tag{30}$$

where μ is the shear modulus and K is the compression modulus due to lattice distortions. Considering the motion of ions around their lattice nodes, Ogata and Ichimaru [87] calculated the shear modulus of the body-centered cubic (bcc) Coulomb crystal. The shear modulus μ is given by

$$\mu = 0.1194\frac{n_i(Ze)^2}{a}, \tag{31}$$

where n_i is the ion number density, $a = [3/(4\pi n_i)]^{1/3}$ is the average ion spacing, and $+Ze$ is the ion charge. Dependence of μ on temperature has been discussed by Strohmayer et al. [88]. The shear modulus can be rewritten as

$$\mu = 0.1194\frac{n_i(Ze)^2}{[1 + 1.781\times(100/\beta)^2]\,a}, \tag{32}$$

where $\beta = (Ze)^2/(ak_{\rm B}T)$, $k_{\rm B}$ is the Boltzmann's constant, and the crystallization point occurs at $\beta = 173$ [89]. We find that the effective shear modulus decreases with an increasing temperature. Horowitz and Hughto [90] calculated the shear modulus of the Coulomb crystal, taking into account weak electron screening in the Thomas–Fermi model. The quantum effects of Coulomb crystal elastic moduli were studied by Baiko [91].

On the other hand, quark matter may form the crystalline CSC phase at the core of NSs [8]. Mannarelli et al. [92] calculated the shear modulus of the crystalline CSC quark matter, and it can be written as

$$\mu = 2.47\ \mathrm{MeV/fm^3}\left(\frac{\Delta}{10\,\mathrm{MeV}}\right)^2\left(\frac{\mu_{\rm q}}{400\,\mathrm{MeV}}\right)^2, \tag{33}$$

where Δ is the gap parameter, which is in the range of 5–25 MeV. For quark matter inside compact stars, the quark chemical potential $\mu_{\rm q}$ range in 350 MeV $< \mu_{\rm q} <$ 500 MeV [92,93]. Taking into account the uncertainty in the gap parameter Δ and in the quark chemical potential $\mu_{\rm q}$, the value of shear modulus is larger than in the conventional NS crust and it is in the range of $7 \times 10^{32}\,{\rm erg\,cm^{-3}}$–$4 \times 10^{34}\,{\rm erg\,cm^{-3}}$.

In essence, the shear modulus μ is determined by the interaction between particles inside matter. That is, $\mu \propto Z^2 e^2 n_i / a \sim \alpha n_i^{4/3}$, where α is the coupling constant. For the SS model, the number density $n_{\rm s}$ of strangeon is much larger than n_i of the NS's crust and the strong interaction dominates over the Coulomb interaction by several orders of magnitude. It can be estimated that the shear modulus of the SS ranges from $10^{32}\,{\rm erg\,cm^{-3}}$ to $10^{34}\,{\rm erg\,cm^{-3}}$ [6,26,27].

5. Asteroseismology of Compact Stars

In Section 5.1, we summarize the perturbation equations for determining the radial oscillation modes and discuss the dynamical stability of compact stars. We discuss the significance of the f-mode as well as present the universal relation connecting the f-mode and the tidal Love number for compact stars in Section 5.2. In Section 5.3, we review the torsional oscillations of compact stars which are thought to be important for the interpretation of QPOs observed in magnetars.

5.1. Dynamical Stability of Compact Stars

Following Li et al. [78], we adopt the radial displacement of a fluid element as $\delta r(r,t)$ and its harmonic oscillation mode with circular frequency ω as $\delta r(r,t) = X(r)e^{i\omega t}$. In practice, we defined a new variable $\zeta = r^2 e^{-\Phi} X$, and thus, the perturbation equation is written as

$$\frac{\mathrm{d}}{\mathrm{d}r}\left(\mathcal{P}\frac{\mathrm{d}\zeta}{\mathrm{d}r}\right) + (\mathcal{Q} + \omega^2 \mathcal{W})\zeta = 0\,, \tag{34}$$

where

$$\begin{aligned} r^2\mathcal{P} &= \Gamma P\, e^{(\Lambda+3\Phi)}\,, \\ r^2\mathcal{Q} &= e^{(\Lambda+3\Phi)}(\rho+P)\left[(\Phi')^2 + 4\frac{\Phi'}{r} - 8\pi e^{2\Lambda}P\right], \\ r^2\mathcal{W} &= (\rho+P)e^{(3\Lambda+\Phi)}\,. \end{aligned} \tag{35}$$

By setting $\eta = \mathcal{P}\zeta'$, one obtains the following coupled differential equations,

$$\frac{\mathrm{d}\zeta}{\mathrm{d}r} = \frac{\eta}{\mathcal{P}}\,, \tag{36}$$

$$\frac{\mathrm{d}\eta}{\mathrm{d}r} = -(\omega^2\mathcal{W} + \mathcal{Q})\zeta\,. \tag{37}$$

At the center of the star, the boundary condition is $3\zeta_0 = \eta_0/\mathcal{P}_0$, where ζ_0 and η_0 are the values of ζ and η at $r = 0$, respectively [94]. By setting $\eta_0 = 1$, we have $\zeta_0 = 1/3\mathcal{P}_0$, where $\mathcal{P}_0 = \Gamma P(0) e^{(\Lambda(0)+3\Phi(0))}$. At the star surface $r = R$, the pressure perturbation must vanish, namely $\Delta P = 0$, which provides another boundary condition, $\Gamma P\zeta' = 0$. Equations (36) and (37) with the above two boundary conditions form a two-point boundary value problem of the Sturm–Liouville type with eigenvalues $\omega_0^2 < \omega_1^2 < \omega_2^2 < \cdots$ [95], where ω_0 is the eigenfrequency of the fundamental mode. If $\omega_0^2 > 0$, all eigenfrequencies of the oscillation modes are real, implying the dynamic stability of the equilibrium stellar model [96–98]. Inversely, $\omega_0^2 < 0$ corresponds to an exponentially growing, unstable radial oscillation. In particular, if the perturbed star is spherically symmetric, the gravitational field in the exterior is static. In other words, a star undergoing radial oscillations does not emit GWs.

In Figure 5, we show the fundamental mode frequencies, ν_0, and the frequencies of the first two excited modes, ν_1 and ν_2, versus the central density for NSs and QSs [78]. The period of the fundamental mode is given by $\tau_0 = 1/\nu_0 = 2\pi/\omega_0$, where ν_0 is the ordinary or temporal frequency. As the central density of the star the frequency of the fundamental mode decreases. It passes through zero at the point at which the mass reaches an extremum. It is worth noting that the frequencies of QSs behave very differently from those of NSs at low central density, rooted in the self-bound and gravity-bound nature of QSs and NSs respectively. Figure 6 displays similar results for self-bound SSs and QSs.

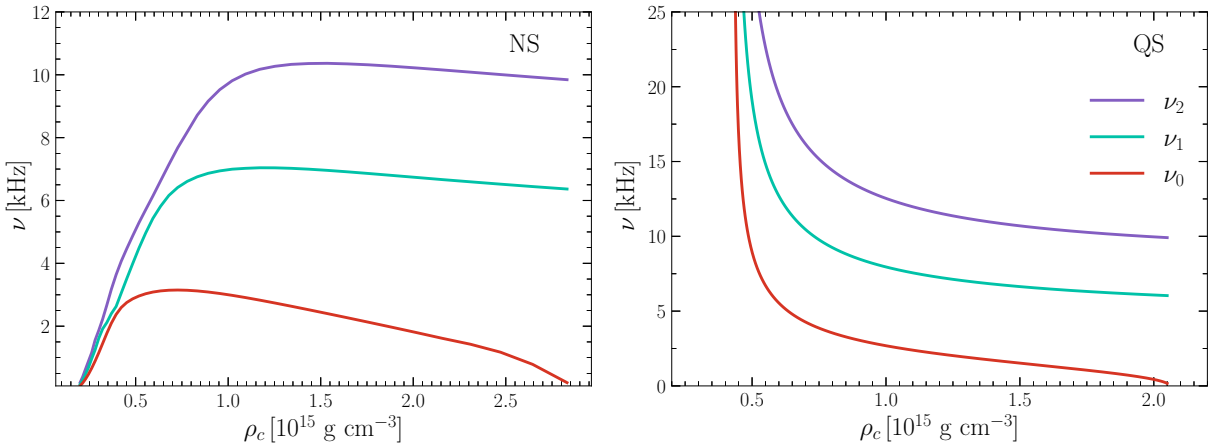

Figure 5. Frequencies of the fundamental mode, ν_0, and the first two excited modes, ν_1 and ν_2, of radial oscillation, as functions of the central density ρ_c. The left panel is NS model, and the right panel is QS model (see Figure 4 in Li et al. [78]).

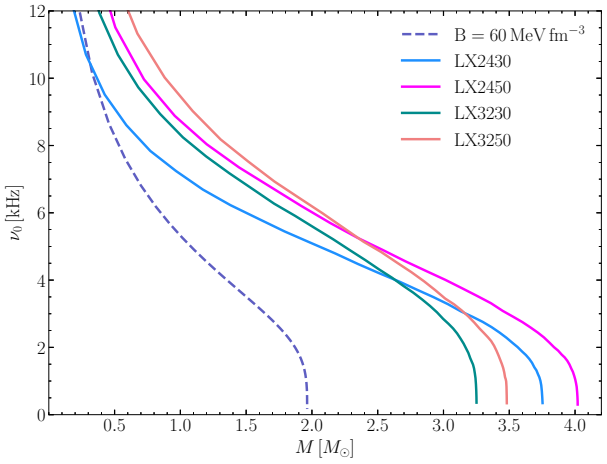

Figure 6. Relationship between the frequencies of the fundamental mode ν_0 and the mass M for QSs and SSs (see Figure 5 in Li et al. [78]).

In examining different results for NSs, QSs, and SSs, it is noteworthy that at low central density, the star can be treated as a homogeneous nonrelativistic star [95]. In this case, the angular frequency ω_0 of the fundamental mode is given by $\omega_0^2 = 4\pi\rho(4\Gamma - 3)/3$. Using the relations between the adiabatic index and the density shown in the lower panel in Figure 2, we expect the frequency ω_0 to diverge as the density reaches a minimum for QSs and SSs. In contrast, for NSs, ω_0 gradually tends toward zero as the central density decreases, with the adiabatic index showing less variation in this scenario.

5.2. Spheroidal Oscillations of Compact Stars

In this subsection, we will introduce the spheroidal oscillation of a relativistic fluid star in the Cowling approximation, which neglects the perturbations of spacetime [99]. The fluid Lagrangian displacement vector is given by

$$\xi^i = \left(e^{-\Lambda}W, -V\partial_\theta, -V\sin^{-2}\theta\partial_\phi\right)r^{-2}Y_{\ell m}(\theta,\phi)\,, \tag{38}$$

where W and V are functions of t and r, while $Y_{\ell m}(\theta,\phi)$ is the spherical harmonic function. Then the perturbation of the four-velocity, δu^μ, can be written as

$$\delta u^\mu = \left(0, e^{-\Lambda}\partial_t W, -\partial_t V\partial_\theta, -\partial_t V\sin^{-2}\theta\partial_\phi\right)r^{-2}e^{-\Phi}Y_{\ell m}(\theta,\phi)\,. \tag{39}$$

Assuming a harmonic time dependence, the perturbative variables can be expressed as $W(t,r) = W(r)e^{i\omega t}$ and $V(t,r) = V(r)e^{i\omega t}$. The final perturbation equations are [100],

$$\frac{\mathrm{d}W}{\mathrm{d}r} = \frac{\mathrm{d}\rho}{\mathrm{d}P}\left[\omega^2 r^2 e^{\Lambda-2\Phi}V + \frac{\mathrm{d}\Phi}{\mathrm{d}r}W\right] - \ell(\ell+1)e^{\Lambda}V\,, \tag{40}$$

$$\frac{\mathrm{d}V}{\mathrm{d}r} = 2\frac{\mathrm{d}\Phi}{\mathrm{d}r}V - e^{\Lambda}\frac{W}{r^2}\,. \tag{41}$$

The boundary condition at the center of the star can be parameterized as, $W = Ar^{l+1}$ and $V = -Ar^l/l$, with A being an arbitrary constant. It can be obtained by examining the behavior of W and V in the vicinity of $r = 0$. At the surface of the star, the perturbed pressure must vanish, which provides

$$\omega^2 e^{\Lambda(R)-2\Phi(R)}V(R) + \frac{1}{R^2}\frac{\mathrm{d}\Phi}{\mathrm{d}r}\Big|_{r=R}W(R) = 0\,. \tag{42}$$

In particular, we consider a uniform-density star; the frequency is given by

$$\omega^2 = \frac{2\ell(\ell-1)}{2\ell+1}\frac{GM}{R^3} \approx 1.5\times10^8\,\frac{2\ell(\ell-1)}{2\ell+1}M_{1.4}R_{10}^3\,s^{-2}\,, \tag{43}$$

where $M_{1.4} = M/1.4\,M_\odot$ and $R_{10} = R/(10\,\mathrm{km})$. This is a reasonable approximation also for a more realistic EOS, and we find that the quadrupole ($\ell = 2$) f-mode has a frequency of approximately 2 kHz [39].

Moreover, the quadrupole f-mode holds significance for several reasons: (i) its behavior is depends on the EOS of compact stars; (ii) it is anticipated to be stimulated in various astrophysical scenarios, leading to efficient GW emission; (iii) its frequency is lower than that of other typical modes, such as p-modes and w-modes, making the f-mode oscillation more likely to be detectable, especially with third-generation detectors like the Einstein Telescope and the Cosmic Explorer [101–103], or conceivably even by the current generation LIGO/Virgo/KAGRA detectors in optimal cases [104–106].

For binary NSs of masses M_a and M_b, the dimensionless tidal coupling constant is defined as [107–109],

$$\kappa_2^t = 2\left[q\left(\frac{X_a}{C_a}\right)^5 k_2^a + \frac{1}{q}\left(\frac{X_b}{C_b}\right)^5 k_2^b\right]\,, \tag{44}$$

where $q = M_b/M_a \le 1$, $X_a = M_a/(M_a+M_b)$, and C_i and k_2^i ($i = a, b$) are respectively the compactness and the quadrupole Love number of each star. In the context of a binary system characterized by a non-rotating, equal-mass configuration, the dimensionless tidal coupling constant can be expressed as follows: $\kappa_2^t = k_2/8C^5 = 3\Lambda/16$, where Λ represents the dimensionless tidal deformability.

Motivated by the universal relation between the dimensionless tidal coupling constant and the f-mode frequency [110], we illustrate the connection between Mf_2 and κ_2^t for NSs,

QSs, and SSs in Figure 7. For NSs and QSs, we observe that the scaled frequency of the f-mode approximately adheres to the following relation:

$$Mf_2 = 0.184(\kappa_2^t)^{-0.016} - 0.154\,. \tag{45}$$

For SSs, the universal relation is

$$Mf_2 = 0.071(\kappa_2^t)^{-0.266}\,. \tag{46}$$

The universal relations for QSs and SSs will complement that of NSs, and play a role in GW data analysis [111].

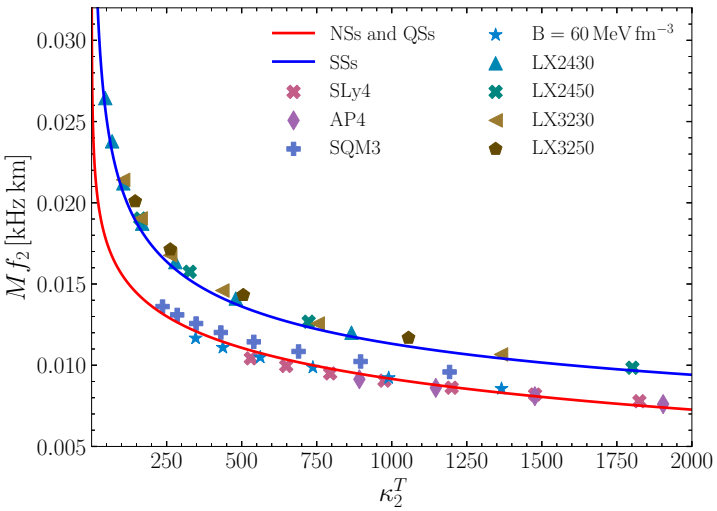

Figure 7. Scaled frequency of the f-mode Mf_2 as a function of the tidal quadrupolar ($l = 2$) coupling constant κ_2^t for NSs, QSs and SSs. The solid line represents the best power-law fit in κ_2^t to the scaled frequencies of the NSs, QSs, and SSs (see Figure 10 in Li et al. [78]).

5.3. Torsional Oscillations of Compact Stars

Torsional oscillations are commonly employed to explain the origin of QPOs observed in the spectra of SGRs [11,12,112–114]. We first consider the torsional oscillations of a non-magnetized relativistic star with axial perturbations. The perturbation equations for the elastic solid star in the Cowling approximation are written as

$$\frac{\mathrm{d}^2 Y}{\mathrm{d}r^2} + \left(\frac{4}{r} + \frac{\mathrm{d}\Phi}{\mathrm{d}r} - \frac{\mathrm{d}\Lambda}{\mathrm{d}r} + \frac{1}{\mu}\frac{\mathrm{d}\mu}{\mathrm{d}r}\right)\frac{\mathrm{d}Y}{\mathrm{d}r} + \left[\frac{\rho + P}{\mu}\omega^2 \mathrm{e}^{-2\Phi} - \frac{(\ell+2)(\ell-1)}{r^2}\right]\mathrm{e}^{2\Lambda} Y = 0\,. \tag{47}$$

Here, $Y(r)$ is the radial component of the angular oscillation amplitude, and the integer ℓ represents the angular separation constant, which comes into play when expanding $Y(r)$ in spherical harmonics $Y_{\ell m}(\theta, \phi)$. To determine the oscillation frequencies, the boundary conditions require that the traction vanishes at the top and the bottom of the crust.

For NS models, we neglect the effects of the magnetic field, superfluid, and nuclear pasta phases in the inner crust. The frequency of the fundamental crust mode corresponding to $n = 0$, is approximately given by [113]

$${}_\ell f_0^2 \approx \frac{e^{2\Phi} v_S^2 (\ell - 1)(\ell + 2)}{2RR_c}\,, \tag{48}$$

where $v_S = (\mu/\rho)^{1/2}$ is the shear speed and R_c is the base of the crust. In particular, matching the observed data of the SGRs with specific crust modes requires a dependence on ℓ. The frequencies of overtone $n > 0$ are given by

$$_{\ell}f_n = e^{\Phi-\Lambda}\frac{n\pi v_S}{\Delta}, \tag{49}$$

where $\Delta = R - R_c$. We find that the frequencies of the overtone are independent of ℓ. For a realistic crust model, the crust thickness can be estimated as follows:

$$\frac{\Delta}{R} \approx \left(1 + \frac{M}{\alpha R}e^{2\Lambda}\right)^{-1}, \tag{50}$$

where the parameter $\alpha = 0.02326$ depends on the EOS of the NS [113].

We explore potential effects of the magnetic field on the frequencies of different torsional modes. In the presence of magnetic fields, the frequencies experience shifts, as described by [114].

$$_{\ell}f_n = {}_{\ell}f_n^{(0)}\left[1 + {}_{\ell}\alpha_n\left(\frac{B}{B_\mu}\right)^2\right]^{1/2}. \tag{51}$$

For NSs models, we chose the EOS WFF3 [115], which describe the core of neutron stars. We consider two different proposed EOSs for the crusts, including EOSs for NV [116] and DH [117] models. We match various core EOSs to two different EOSs for the crust. The crust–core boundary for the NV and DH EOSs is defined at $\rho \approx 2.4 \times 10^{14}\,\mathrm{g\,cm^{-3}}$, and $\rho \approx 1.28 \times 10^{14}\,\mathrm{g\,cm^{-3}}$, respectively.

In Figure 8, we show the effects of the magnetic field on the oscillation frequencies of NSs. The magnetic field strength is normalized by $B_\mu = 4 \times 10^{15}$ G. The various dashed lines in Figure 8 represent our fits to the numerically calculated data with high accuracy. In the case of $B > B_\mu$, we observe that the frequencies exhibit a quadratic growth concerning the magnetic field and tend to display reduced sensitivity to NS parameters.

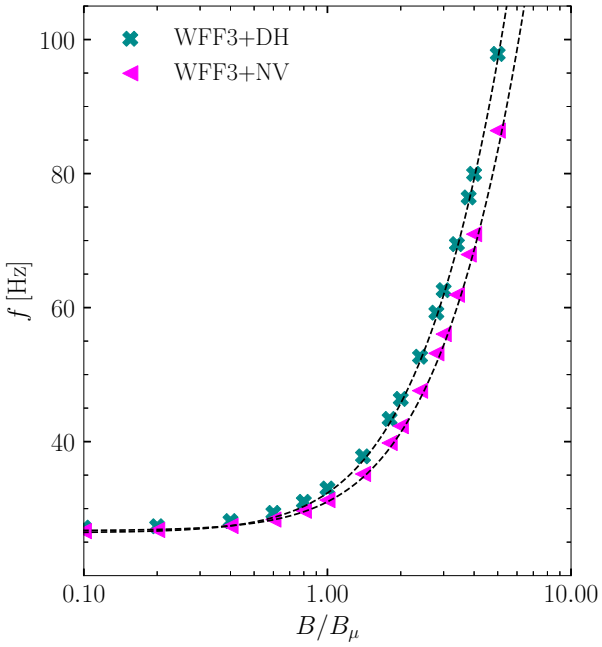

Figure 8. The frequencies of the fundamental mode $n = 0$ and $\ell = 2$ torsional mode frequencies as a function of the magnetic field. The NS mass is chosen as $M = 1.4\,M_\odot$. The dashed lines correspond to our fits using the empirical formula (51) with different coefficient values. The fitting values are 0.5 and 0.35 for WFF3+ DH model and WFF3+ NV model, respectively.

Alternatively, involving strange quarks may shed light on the physical mechanism of QPOs in GFs. In our recent work [27], we systematically investigate torsional oscillation frequencies based on the SS model. The fundamental frequencies of the $\ell = 2$ mode vary from 145 Hz to 277 Hz, depending on the SS mass. For the case of the first overtone $_{\ell}f_1$, the

frequencies range from 300 Hz to 1700 Hz and the first overtone frequency decreases as the SS mass increases (see Tables 1, 2, and 3 of Li et al. [27]). However, such an anticorrelation differs from those of NSs, where the frequency of the first overtone would increase with a higher NS mass [114]. In particular, our results explain well the high-frequency QPOs ($\gtrsim$150 Hz).

Due to the higher shear modulus of the SS model, explaining the low-frequency QPOs ($\lesssim$150 Hz) becomes challenging. Consequently, we suggest the possibility that SSs may possess a thin surface ocean characterized by density and temperature within the ranges of 10^6–10^9 g cm^{-3} and 10^8–10^9 K, respectively. With the presence of such an ocean layer, we can employ the interface modes at the ocean–crust interface to account for the low-frequency QPOs. The frequency of the interface mode can be analytically approximated as [118]

$$f \approx 16.5\,\mathrm{Hz}\left(\frac{\beta}{173}\right)^{1/2}\left(\frac{T_8}{4}\right)^{1/2} \times \left(\frac{64}{A}\right)^{1/2}\left(\frac{10\ \mathrm{km}}{R}\right)\left[\frac{\ell(\ell+1)}{2}\right]^{1/2}, \tag{52}$$

where $T_8 \equiv T/10^8$K, and A is the baryon number. We estimate the frequencies of the ocean–crust interface modes and observe that these modes provide a suitable interpretation for the observed low-frequency QPOs in GFs for some SGRs.

In Figure 9, we show the effects of the magnetic field on the torsional modes for the SS model. The magnetic field strength is normalized by $B_\mu = 4 \times 10^{16}$ G. The various dashed lines in Figure 9 represent our fits to the numerically calculated data. In the case of $B > B_\mu$, we observe that the frequencies exhibit a quadratic growth concerning the magnetic field and tend to display reduced sensitivity to the SS parameters. NSs could exhibit similar behaviors, but the critical magnetic field strength for this transition is much lower, approximately $\sim 4 \times 10^{15}$ G [114].

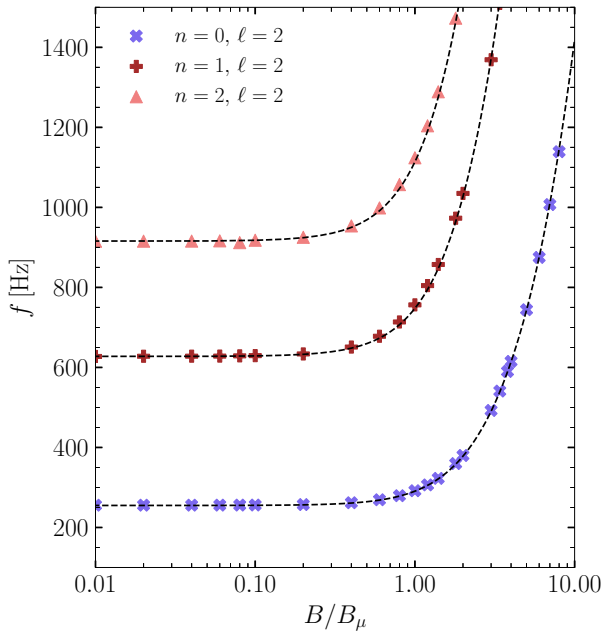

Figure 9. Frequencies of different overtones as a function of the normalized magnetic field for $\ell = 2$ (see Figure 3 in Li et al. [27]). The dashed lines are our fits using Equation (51). The SS mass is chosen as $M = 1.4\,M_\odot$. The coefficients ${}_\ell\alpha_n$ are 0.3, 0.42 and 0.48 for $n = 0$, $n = 1$, and $n = 2$, respectively.

6. Summary

The EOS serves as a tool for deducing crucial aspects of microphysics, including the characteristics of nucleon interaction and the potential existence of free quarks at high densities. Therefore, determining the EOS of supranuclear density matter holds significant importance in fundamental physics. We focus in detail on how to constrain the EOS of

compact stars induced by asteroseismology. Observations that include studies of QPOs in GFs and GWs provide information about the elastic properties and internal compositions of compact stars.

The dynamical stability of stellar configurations for radial perturbations is determined by the fundamental mode. In this review, we have investigated the properties of radial oscillations of compact stars in detail and study the stability of compact stars rigorously. We find that the fundamental mode frequency of the models of the self-bound on the surface by strong interaction (e.g.,QSs and SSs) is very different from that of the gravity-bound model (NSs) at low central density. This can be understood by approximating the stars in the nonrelativistic regime and observing that the adiabatic index Γ for the self-bound models tends to infinity as the density decreases to its minimum value. The presence of this elastic property of quark matter in the core should produce astrophysical signatures that are different from those of normal NSs with a fluid core. Pereira et al. [59] investigated the dynamical stability of HSs with elastic quark phases. In particular, the imprint of elasticity on the eigenfrequencies is mostly relevant for large masses and the relative changes would be larger than 10% for NSs with mass above $2\,M_{\odot}$. We will discuss the effect of the elastic property on the dynamical stability of SSs in the future.

The frequencies of torsional oscillations are highly dependent on the elastic properties. In the SS model, we observe its ability to accurately describe the high-frequency QPOs in the GFs of some SGRs. Additionally, we explore the impact of magnetic fields on the frequencies of torsional oscillations. The typical value of the magnetic field strength is adopted as $B_{\mu} = 4 \times 10^{16}\,\mathrm{G}$, which is much larger than the ordinary NS models. Alcock et al. [119] suggested that QSs could have a thin nuclear crust that extends to the neutron drip density (i.e., $\rho \approx 4 \times 10^{11}\,\mathrm{g\,cm^{-3}}$). Jaikumar et al. [120] proposed another possible model that a crust is made up of nuggets of strange quark matter embedded in a uniform electron background. Our results show that both models are difficult to reproduce the recorded QPO frequencies well [27].

Author Contributions: Conceptualization, H.-B.L., Y.G., L.S. and R.-X.X. All authors have read and agreed to the published version of the manuscript.

Funding: This work was supported by the National SKA Program of China (2020SKA0120300, 2020SKA0120100), the National Natural Science Foundation of China (11975027, 11991053, 11721303), the Beijing Natural Science Foundation (1242018), the Max Planck Partner Group Program funded by the Max Planck Society, the Strategic Priority Research Program of CAS (No. XDB0550300), and the High-Performance Computing Platform of Peking University.

Data Availability Statement: The data underlying this paper will be shared on reasonable request to the corresponding authors.

Conflicts of Interest: The authors declare no conflicts of interest.

References

1. Oertel, M.; Hempel, M.; Klähn, T.; Typel, S. Equations of state for supernovae and compact stars. *Rev. Mod. Phys.* **2017**, *89*, 015007. [CrossRef]
2. Baym, G.; Hatsuda, T.; Kojo, T.; Powell, P.D.; Song, Y.; Takatsuka, T. From hadrons to quarks in neutron stars: A review. *Rept. Prog. Phys.* **2018**, *81*, 056902. [CrossRef]
3. Annala, E.; Gorda, T.; Hirvonen, J.; Komoltsev, O.; Kurkela, A.; Nättilä, J.; Vuorinen, A. Strongly interacting matter exhibits deconfined behavior in massive neutron stars. *Nat. Commun.* **2023**, *14*, 8451. [CrossRef] [PubMed]
4. Glendenning, N.K. *Compact Stars: Nuclear Physics, Particle Physics, and General Relativity*; Springer: New York, NY, USA, 2000.
5. Witten, E. Cosmic Separation of Phases. *Phys. Rev. D* **1984**, *30*, 272–285. [CrossRef]
6. Xu, R.X. Solid quark matter? *Astrophys. J.* **2003**, *596*, L59–L62. [CrossRef]
7. Haensel, P.; Potekhin, A.Y.; Yakovlev, D.G. *Neutron Stars 1: Equation of State and Structure*; Springer: New York, NY, USA, 2007; Volume 326. [CrossRef]
8. Alford, M.; Braby, M.; Paris, M.W.; Reddy, S. Hybrid stars that masquerade as neutron stars. *Astrophys. J.* **2005**, *629*, 969–978. [CrossRef]
9. Zhang, C.; Gao, Y.; Xia, C.J.; Xu, R. Hybrid strangeon stars. *Phys. Rev. D* **2023**, *108*, 123031. [CrossRef]
10. Xu, R.X.; Qiao, G.J.; Zhang, B. Psr 0943+10: A bare strange star? *Astrophys. J.* **1999**, *522*, L109. [CrossRef]

11. Duncan, R.C. Global seismic oscillations in soft gamma repeaters. *Astrophys. J.* **1998**, *498*, L45. [CrossRef]
12. Strohmayer, T.E.; Watts, A.L. Discovery of fast X-ray oscillations during the 1998 giant flare from SGR 1900+14. *Astrophys. J.* **2005**, *632*, L111–L114. [CrossRef]
13. Ushomirsky, G.; Cutler, C.; Bildsten, L. Deformations of accreting neutron star crusts and gravitational wave emission. *Mon. Not. R. Astron. Soc.* **2000**, *319*, 902. [CrossRef]
14. Haskell, B.; Jones, D.I.; Andersson, N. Mountains on Neutron Stars: Accreted vs. Non-Accreted crusts. *Mon. Not. R. Astron. Soc.* **2006**, *373*, 1423–1439. [CrossRef]
15. Haskell, B.; Patruno, A. Are Gravitational Waves Spinning Down PSR J1023+0038? *Phys. Rev. Lett.* **2017**, *119*, 161103. [CrossRef]
16. Johnson-McDaniel, N.K.; Owen, B.J. Maximum elastic deformations of relativistic stars. *Phys. Rev. D* **2013**, *88*, 044004. [CrossRef]
17. Abbott, B.P.; Abbott, R.; Abbott, T.D.; Abraham, S.; Acernese, F.; Ackley, K.; Adams, C.; Adhikari, R.X.; Adya, V.B.; Affeldt, C.; et al. Searches for Gravitational Waves from Known Pulsars at Two Harmonics in 2015–2017 LIGO Data. *Astrophys. J.* **2019**, *879*, 10; Erratum in *Astrophys. J.* **2020**, *899*, 170. [CrossRef]
18. Ruderman, M. Neutron Starquakes and Pulsar Periods. *Nature* **1969**, *223*, 597–598. [CrossRef]
19. Anderson, P.W.; Itoh, N. Pulsar glitches and restlessness as a hard superfluidity phenomenon. *Nature* **1975**, *256*, 25–27. [CrossRef]
20. Alpar, M.A.; Anderson, P.W.; Pines, D.; Shaham, J. Giant glitches and pinned vorticity in the VELA and other pulsars. *Astrophys. J.* **1981**, *249*, L29–L33. [CrossRef]
21. Antonelli, M.; Montoli, A.; Pizzochero, P. *Insights into the Physics of Neutron Star Interiors from Pulsar Glitches*; World Scientific: Singapore, 2023. [CrossRef]
22. Antonopoulou, D.; Haskell, B.; Espinoza, C.M. Pulsar glitches: Observations and physical interpretation. *Rept. Prog. Phys.* **2022**, *85*, 126901. [CrossRef]
23. Zhou, A.Z.; Xu, R.X.; Wu, X.J.; Wang, N.; Hong, X.Y. Quakes in solid quark stars. *Astropart. Phys.* **2004**, *22*, 73–79. [CrossRef]
24. Lai, X.Y.; Yun, C.A.; Lu, J.G.; Lü, G.L.; Wang, Z.J.; Xu, R.X. Pulsar Glitches in a Strangeon Star Model. *Mon. Not. R. Astron. Soc.* **2018**, *476*, 3303–3309. [CrossRef]
25. Wang, W.; Lai, X.; Zhou, E.; Lu, J.; Zheng, X.; Xu, R. Pulsar glitches in a strangeon star model—II. The activity. *Mon. Not. R. Astron. Soc.* **2020**, *500*, 5336–5349. [CrossRef]
26. Lai, X.Y.; Wang, W.H.; Yuan, J.P.; Lu, R.P.; Yue, H.; Xu, R.X. Pulsar glitch in a strangeon star model—III. The recovery. *Mon. Not. R. Astron. Soc.* **2023**, *523*, 3967–3973. [CrossRef]
27. Li, H.B.; Kang, Y.; Hu, Z.; Shao, L.; Xia, C.J.; Xu, R.X. Quasi-periodic oscillations during magnetar giant flares in the strangeon star model. *Mon. Not. R. Astron. Soc.* **2023**, *527*, 855–862. [CrossRef]
28. Antoniadis, J.; Freire, P.C.; Wex, N.; Tauris, T.M.; Lynch, R.S.; Van Kerkwijk, M.H.; Kramer, M.; Bassa, C.; Dhillon, V.S.; Driebe, T.; et al. A Massive Pulsar in a Compact Relativistic Binary. *Science* **2013**, *340*, 6131. [CrossRef]
29. Fonseca, E.; Cromartie, H.T.; Pennucci, T.T.; Ray, P.S.; Kirichenko, A.Y.; Ransom, S.M.; Demorest, P.B.; Stairs, I.H.; Arzoumanian, Z.; Guillemot, L.; et al. Refined Mass and Geometric Measurements of the High-mass PSR J0740+6620. *Astrophys. J. Lett.* **2021**, *915*, L12. [CrossRef]
30. Gendreau, K.C.; Arzoumanian, Z.; Adkins, P.W.; Albert, C.L.; Anders, J.F.; Aylward, A.T.; Baker, C.L.; Balsamo, E.R.; Bamford, W.A.; Benegalrao, S.S.; et al. The Neutron star Interior Composition Explorer (NICER): Design and development. In *Proceedings of the Space Telescopes and Instrumentation 2016: Ultraviolet to Gamma Ray*; Society of Photo-Optical Instrumentation Engineers (SPIE) Conference Series; den Herder, J.W.A., Takahashi, T., Bautz, M., Eds.; SPIE: Bellingham, WA, USA, 2016; Volume 9905, p. 99051H. [CrossRef]
31. Baubock, M.; Psaltis, D.; Ozel, F. Effects of Spot Size on Neutron-Star Radius Measurements from Pulse Profiles. *Astrophys. J.* **2015**, *811*, 144. [CrossRef]
32. Miller, M.C. The Case for psr J1614–2230 as a Nicer Target. *Astrophys. J.* **2016**, *822*, 27. [CrossRef]
33. Özel, F.; Freire, P. Masses, Radii, and the Equation of State of Neutron Stars. *Ann. Rev. Astron. Astrophys.* **2016**, *54*, 401–440. [CrossRef]
34. Bogdanov, S.; Grindlay, J.E.; Rybicki, G.B. Thermal X-rays from Millisecond Pulsars: Constraining the Fundamental Properties of Neutron Stars. *Astrophys. J.* **2008**, *689*, 407. [CrossRef]
35. Watts, A.L.; Andersson, N.; Chakrabarty, D.; Feroci, M.; Hebeler, K.; Israel, G.; Lamb, F.K.; Miller, M.C.; Morsink, S.; Özel, F.; et al. Colloquium: Measuring the neutron star equation of state using X-ray timing. *Rev. Mod. Phys.* **2016**, *88*, 021001. [CrossRef]
36. Haskell, B.; Bejger, M. Astrophysics with continuous gravitational waves. *Nat. Astron.* **2023**, *7*, 1160–1170. [CrossRef]
37. Abbott, B.P.; Abbott, R.; Abbott, T.; Acernese, F.; Ackley, K.; Adams, C.; Adams, T.; Addesso, P.; Adhikari, R.X.; Adya, V.B.; et al. GW170817: Observation of Gravitational Waves from a Binary Neutron Star Inspiral. *Phys. Rev. Lett.* **2017**, *119*, 161101. [CrossRef]
38. Yunes, N.; Miller, M.C.; Yagi, K. Gravitational-wave and X-ray probes of the neutron star equation of state. *Nat. Rev. Phys.* **2022**, *4*, 237–246. [CrossRef]
39. Andersson, N. Gravitational waves from instabilities in relativistic stars. *Class. Quant. Grav.* **2003**, *20*, R105. [CrossRef]
40. Andersson, N.; Ferrari, V.; Jones, D.I.; Kokkotas, K.D.; Krishnan, B.; Read, J.S.; Rezzolla, L.; Zink, B. Gravitational waves from neutron stars: Promises and challenges. *Gen. Rel. Grav.* **2011**, *43*, 409–436. [CrossRef]
41. Kokkotas, K.D.; Schutz, B.F. W-modes: A New family of normal modes of pulsating relativistic stars. *Mon. Not. R. Astron. Soc.* **1992**, *255*, 119. [CrossRef]
42. McDermott, P.N.; van Horn, H.M.; Hansen, C.J. Nonradial Oscillations of Neutron Stars. *Astrophys. J.* **1988**, *325*, 725. [CrossRef]

43. Annala, E.; Gorda, T.; Kurkela, A.; Nättilä, J.; Vuorinen, A. Evidence for quark-matter cores in massive neutron stars. *Nat. Phys.* **2020**, *16*, 907–910. [CrossRef]
44. Paschalidis, V.; Yagi, K.; Alvarez-Castillo, D.; Blaschke, D.B.; Sedrakian, A. Implications from GW170817 and I-Love-Q relations for relativistic hybrid stars. *Phys. Rev. D* **2018**, *97*, 084038. [CrossRef]
45. Zhou, E.P.; Zhou, X.; Li, A. Constraints on interquark interaction parameters with GW170817 in a binary strange star scenario. *Phys. Rev. D* **2018**, *97*, 083015. [CrossRef]
46. Miao, Z.; Li, A.; Zhu, Z.; Han, S. Constraining hadron-quark phase transition parameters within the quark-mean-field model using multimessenger observations of neutron stars. *Astrophys. J.* **2020**, *904*, 103. [CrossRef]
47. Yu, H.; Weinberg, N.N. Dynamical tides in coalescing superfluid neutron star binaries with hyperon cores and their detectability with third generation gravitational-wave detectors. *Mon. Not. Roy. Astron. Soc.* **2017**, *470*, 350–360. [CrossRef]
48. Lau, S.Y.; Yagi, K. Probing hybrid stars with gravitational waves via interfacial modes. *Phys. Rev. D* **2021**, *103*, 063015. [CrossRef]
49. Zhu, J.; Wang, C.; Xia, C.; Zhou, E.; Ma, Y. Probing phase transitions in neutron stars via the crust-core interfacial mode. *Phys. Rev. D* **2023**, *107*, 083023. [CrossRef]
50. Zavlin, V.E.; Pavlov, G.G. Modeling neutron star atmospheres. In Proceedings of the 270th WE-Heraeus Seminar on Neutron Stars, Pulsars and Supernova Remnants, Bad Honnef, Germany, 21–25 January 2002; pp. 262–272.
51. Potekhin, A.Y. Atmospheres and radiating surfaces of neutron stars. *Phys. Usp.* **2014**, *57*, 735–770. [CrossRef]
52. Baym, G.; Pethick, C.; Sutherland, P. The Ground State of Matter at High Densities: Equation of State and Stellar Models. *Astrophys. J.* **1971**, *170*, 299. [CrossRef]
53. Pethick, C.J.; Ravenhall, D.G. Matter at large neutron excess and the physics of neutron-star crusts. *Ann. Rev. Nucl. Part. Sci.* **1995**, *45*, 429–484. [CrossRef]
54. Chamel, N.; Haensel, P. Physics of Neutron Star Crusts. *Living Rev. Rel.* **2008**, *11*, 10. [CrossRef]
55. Rezzolla, L.; Pizzochero, P.; Jones, D.I.; Rea, N.; Vidaña, I. (Eds.) *The Physics and Astrophysics of Neutron Stars*; Springer: Cham, Switzerland, 2018; Volume 457. [CrossRef]
56. Read, J.S.; Lackey, B.D.; Owen, B.J.; Friedman, J.L. Constraints on a phenomenologically parameterized neutron-star equation of state. *Phys. Rev. D* **2009**, *79*, 124032. [CrossRef]
57. Caplan, M.E.; Horowitz, C.J. Colloquium: Astromaterial science and nuclear pasta. *Rev. Mod. Phys.* **2017**, *89*, 041002. [CrossRef]
58. Haskell, B.; Andersson, N.; Jones, D.I.; Samuelsson, L. Are neutron stars with crystalline color-superconducting cores relevant for the LIGO experiment? *Phys. Rev. Lett.* **2007**, *99*, 231101. [CrossRef]
59. Pereira, J.P.; Bejger, M.; Tonetto, L.; Lugones, G.; Haensel, P.; Zdunik, J.L.; Sieniawska, M. Probing elastic quark phases in hybrid stars with radius measurements. *Astrophys. J.* **2021**, *910*, 145. [CrossRef]
60. Lindblom, L. Spectral Representations of Neutron-Star Equations of State. *Phys. Rev. D* **2010**, *82*, 103011. [CrossRef]
61. Bardeen, J.; Cooper, L.N.; Schrieffer, J.R. Microscopic theory of superconductivity. *Phys. Rev.* **1957**, *106*, 162. [CrossRef]
62. Alford, M.G.; Schmitt, A.; Rajagopal, K.; Schäfer, T. Color superconductivity in dense quark matter. *Rev. Mod. Phys.* **2008**, *80*, 1455–1515. [CrossRef]
63. Lin, L.M. Torsional oscillations of crystalline color-superconducting hybrid stars: Possible sources for Advanced LIGO? *Phys. Rev. D* **2013**, *88*, 124002. [CrossRef]
64. Lau, S.Y.; Leung, P.T.; Lin, L.M. Tidal deformations of compact stars with crystalline quark matter. *Phys. Rev. D* **2017**, *95*, 101302. [CrossRef]
65. Lai, X.Y.; Xu, R.X. Quark stars composed of Lennard-Jones matter. *Mon. Not. R. Astron. Soc.* **2009**, *398*, 31. [CrossRef]
66. Lai, X.Y.; Gao, C.Y.; Xu, R.X. H-cluster stars. *Mon. Not. R. Astron. Soc.* **2012**, *431*, 3282–3290. [CrossRef]
67. Lai, X.; Xu, R. Quark-Cluster Stars: The Structure. In *Proceedings of the International Journal of Modern Physics Conference Series*; World Scientific: Singapore, 2013; Volume 23, pp. 213–222. [CrossRef]
68. Xu, R.X. 1E 1207.4-5209: A Low-mass bare strange star? *Mon. Not. R. Astron. Soc.* **2005**, *356*, 359–370. [CrossRef]
69. Yue, Y.L.; Cui, X.H.; Xu, R.X. Is psr b0943+10 a low-mass quark star? *Astrophys. J.* **2006**, *649*, L95–L98. [CrossRef]
70. Zhu, W.W.; Xu, R.X. GCRT J1745-3009: A precessing radio pulsar? *Mon. Not. R. Astron. Soc.* **2006**, *365*, L16. [CrossRef]
71. Lai, X.; Xia, C.; Xu, R. Bulk strong matter: The trinity. *Adv. Phys. X* **2023**, *8*, 2137433. [CrossRef]
72. Wang, W.Y.; Yang, Y.P.; Niu, C.H.; Xu, R.; Zhang, B. Magnetospheric Curvature Radiation by Bunches as Emission Mechanism for Repeating Fast Radio Bursts. *Astrophys. J.* **2022**, *927*, 105. [CrossRef]
73. Wang, W.Y.; Jiang, J.C.; Lu, J.; Xu, H.; Xu, J.; Lee, K.; Liu, J.; Xu, R. Repeating fast radio bursts: Coherent circular polarization by bunches. *Sci. China Phys. Mech. Astron.* **2022**, *65*, 289511. [CrossRef]
74. Lai, X.Y.; Yu, Y.W.; Zhou, E.P.; Li, Y.Y.; Xu, R.X. Merging Strangeon Stars. *Res. Astron. Astrophys.* **2018**, *18*, 024. [CrossRef]
75. Lai, X.Y.; Zhou, E.P.; Xu, R.X. Strangeons constitute bulk strong matter: Test using GW 170817. *Eur. Phys. J. A* **2019**, *55*, 60. [CrossRef]
76. Lai, X.Y.; Xia, C.J.; Yu, Y.W.; Xu, R.X. Merging strangeon stars II: The ejecta and light curves. *Res. Astron. Astrophys.* **2021**, *21*, 250. [CrossRef]
77. Gao, Y.; Lai, X.Y.; Shao, L.; Xu, R.X. Rotation and deformation of strangeon stars in the Lennard-Jones model. *Mon. Not. R. Astron. Soc.* **2022**, *509*, 2758–2779. [CrossRef]
78. Li, H.B.; Gao, Y.; Shao, L.; Xu, R.X.; Xu, R. Oscillation modes and gravitational waves from strangeon stars. *Mon. Not. R. Astron. Soc.* **2022**, *516*, 6172–6179. [CrossRef]

79. Lattimer, J.M.; Prakash, M. Neutron star structure and the equation of state. *Astrophys. J.* **2001**, *550*, 426. [CrossRef]
80. Fantina, A.F.; Chamel, N.; Pearson, J.M.; Goriely, S. Neutron star properties with unified equations of state of dense matter. *Astron. Astrophys.* **2013**, *559*, A128. [CrossRef]
81. Lattimer, J.M.; Prakash, M. The Ultimate energy density of observable cold matter. *Phys. Rev. Lett.* **2005**, *94*, 111101. [CrossRef] [PubMed]
82. Mogliacci, S.; Andersen, J.O.; Strickland, M.; Su, N.; Vuorinen, A. Equation of State of hot and dense QCD: Resummed perturbation theory confronts lattice data. *J. High Energy Phys.* **2013**, *12*, 055. [CrossRef]
83. Fraga, E.S.; Kurkela, A.; Vuorinen, A. Interacting quark matter equation of state for compact stars. *Astrophys. J. Lett.* **2014**, *781*, L25. [CrossRef]
84. Fraga, E.S.; Kurkela, A.; Vuorinen, A. Neutron star structure from QCD. *Eur. Phys. J. A* **2016**, *52*, 49. [CrossRef]
85. Kurkela, A.; Vuorinen, A. Cool quark matter. *Phys. Rev. Lett.* **2016**, *117*, 042501. [CrossRef]
86. Ghiglieri, J.; Kurkela, A.; Strickland, M.; Vuorinen, A. Perturbative Thermal QCD: Formalism and Applications. *Phys. Rept.* **2020**, *880*, 1–73. [CrossRef]
87. Ogata, S.; Ichimaru, S. First-principles calculations of shear moduli for Monte Carlo-simulated Coulomb solids. *Phys. Rev. A* **1990**, *42*, 4867–4870. [CrossRef]
88. Strohmayer, T.; Ogata, S.; Iyetomi, H.; Ichimaru, S.; van Horn, H.M. The Shear Modulus of the Neutron Star Crust and Nonradial Oscillations of Neutron Stars. *Astrophys. J.* **1991**, *375*, 679. [CrossRef]
89. Farouki, R.T.; Hamaguchi, S. Thermal energy of the crystalline one-component plasma from dynamical simulations. *Phys. Rev. E* **1993**, *47*, 4330–4336. [CrossRef] [PubMed]
90. Horowitz, C.J.; Hughto, J. Molecular Dynamics Simulation of Shear Moduli for Coulomb Crystals. *arXiv* **2008**, arXiv:0812.2650.
91. Baiko, D.A. Shear modulus of neutron star crust. *Mon. Not. R. Astron. Soc.* **2011**, *416*, 22. [CrossRef]
92. Mannarelli, M.; Rajagopal, K.; Sharma, R. The Rigidity of crystalline color superconducting quark matter. *Phys. Rev. D* **2007**, *76*, 074026. [CrossRef]
93. Ippolito, N.D.; Nardulli, G.; Ruggieri, M. Self-consistent evaluation of quark masses in three flavor crystalline color superconductivity. *J. High Energy Phys.* **2007**, *04*, 036. [CrossRef]
94. Kokkotas, K.D.; Ruoff, J. Radial oscillations of relativistic stars. *Astron. Astrophys.* **2001**, *366*, 565. [CrossRef]
95. Shapiro, S.L.; Teukolsky, S.A. *Black Holes, White Dwarfs, and Neutron Stars: The Physics of Compact Objects*; Wiley-VCH: New York, NY, USA, 1983.
96. Chandrasekhar, S. Dynamical Instability of Gaseous Masses Approaching the Schwarzschild Limit in General Relativity. *Phys. Rev. Lett.* **1964**, *12*, 114–116. [CrossRef]
97. Chandrasekhar, S. The Dynamical Instability of Gaseous Masses Approaching the Schwarzschild Limit in General Relativity. *Astrophys. J.* **1964**, *140*, 417–433. Erratum in *Astrophys. J.* **1964**, *140*, 1342. [CrossRef]
98. Misner, C.W.; Thorne, K.S.; Wheeler, J.A. *Gravitation*; W. H. Freeman: San Francisco, CA, USA, 1973.
99. Cowling, T.G. The non-radial oscillations of polytropic stars. *Mon. Not. R. Astron. Soc.* **1941**, *101*, 367. [CrossRef]
100. Sotani, H.; Yasutake, N.; Maruyama, T.; Tatsumi, T. Signatures of hadron-quark mixed phase in gravitational waves. *Phys. Rev. D* **2011**, *83*, 024014. [CrossRef]
101. Punturo, M.; Abernathy, M.; Acernese, F.; Allen, B.; Andersson, N.; Arun, K.; Barone, F.; Barr, B.; Barsuglia, M.; Beker, M.; et al. The Einstein Telescope: A third-generation gravitational wave observatory. *Class. Quant. Grav.* **2010**, *27*, 194002. [CrossRef]
102. Sathyaprakash, B.S.; Buonanno, A.; Lehner, L.; Broeck, C.V.D.; Ajith, P.; Ghosh, A.; Chatziioannou, K.; Pani, P.; Puerrer, M.; Sotiriou, T.; et al. Extreme gravity and fundamental physics. *Bull. Am. Astron. Soc.* **2019**, *51*, 251.
103. Kalogera, V.; Sathyaprakash, B.S.; Bailes, M.; Bizouard, M.-A.; Buonanno, A.; Burrows, A.; Colpi, M.; Evans, M.; Fairhurst, S.; Hild, S.; et al. The Next Generation Global Gravitational Wave Observatory: The Science Book. *arXiv* **2021**, arXiv:2111.06990.
104. Abbott, B.P.; Abbott, R.; Abbott, T.D.; Acernese, F.; Ackley, K.; Adams, C.; Adams, T.; Addesso, P.; Adhikari, R.X.; Adya, V.B.; et al. Constraining the *p*-Mode–*g*-Mode Tidal Instability with GW170817. *Phys. Rev. Lett.* **2019**, *122*, 061104. [CrossRef] [PubMed]
105. LIGO Scientific Collaboration; Virgo Collaboration; KAGRA Collaboration; Abbott, R.; Abe, H.; Acernese, F.; Ackley, K.; Adhikari, N.; Adhikari, R.X.; Adkins, V.K.; et al. First joint observation by the underground gravitational-wave detector KAGRA with GEO 600. *Prog. Theor. Exp. Phys.* **2022**, *2022*, 063F01. [CrossRef]
106. Abe, H.; Akutsu, T.; Ando, M.; Araya, A.; Aritomi, N.; Asada, H.; Aso, Y.; Bae, S.; Bajpai, R.; Cannon, K.; et al. The Current Status and Future Prospects of KAGRA, the Large-Scale Cryogenic Gravitational Wave Telescope Built in the Kamioka Underground. *Galaxies* **2022**, *10*, 63. [CrossRef]
107. Bernuzzi, S.; Nagar, A.; Balmelli, S.; Dietrich, T.; Ujevic, M. Quasiuniversal properties of neutron star mergers. *Phys. Rev. Lett.* **2014**, *112*, 201101. [CrossRef]
108. Bernuzzi, S.; Nagar, A.; Dietrich, T.; Damour, T. Modeling the Dynamics of Tidally Interacting Binary Neutron Stars up to the Merger. *Phys. Rev. Lett.* **2015**, *114*, 161103. [CrossRef]
109. Bernuzzi, S.; Dietrich, T.; Nagar, A. Modeling the complete gravitational wave spectrum of neutron star mergers. *Phys. Rev. Lett.* **2015**, *115*, 091101. [CrossRef]
110. Chakravarti, K.; Andersson, N. Exploring universality in neutron star mergers. *Mon. Not. R. Astron. Soc.* **2020**, *497*, 5480–5484. [CrossRef]
111. Shao, L.; Yagi, K. Neutron stars as extreme laboratories for gravity tests. *Sci. Bull.* **2022**, *67*, 1946–1949. [CrossRef] [PubMed]

112. Piro, A.L. Shear waves and giant flare oscillations from soft gamma-ray repeaters. *Astrophys. J.* **2005**, *634*, L153–L156. [CrossRef]
113. Samuelsson, L.; Andersson, N. Neutron Star Asteroseismology. Axial Crust Oscillations in the Cowling Approximation. *Mon. Not. R. Astron. Soc.* **2007**, *374*, 256–268. [CrossRef]
114. Sotani, H.; Kokkotas, K.D.; Stergioulas, N. Torsional Oscillations of Relativistic Stars with Dipole Magnetic Fields. *Mon. Not. R. Astron. Soc.* **2007**, *375*, 261–277. [CrossRef]
115. Wiringa, R.B.; Fiks, V.; Fabrocini, A. Equation of state for dense nucleon matter. *Phys. Rev. C* **1988**, *38*, 1010–1037. [CrossRef] [PubMed]
116. Negele, J.W.; Vautherin, D. Neutron star matter at sub-nuclear densities. *Nucl. Phys. A* **1973**, *207*, 298–320. [CrossRef]
117. Douchin, F.; Haensel, P. A unified equation of state of dense matter and neutron star structure. *Astron. Astrophys.* **2001**, *380*, 151. [CrossRef]
118. Piro, A.L.; Bildsten, L. Neutron star crustal interface waves. *Astrophys. J.* **2005**, *619*, 1054–1063. [CrossRef]
119. Alcock, C.; Farhi, E.; Olinto, A. Strange stars. *Astrophys. J.* **1986**, *310*, 261–272. [CrossRef]
120. Jaikumar, P.; Reddy, S.; Steiner, A.W. The Strange star surface: A Crust with nuggets. *Phys. Rev. Lett.* **2006**, *96*, 041101. [CrossRef] [PubMed]